http://dx.doi.org/10.5012/bkcs.2013.34.9.2765

# Effect of Titanium Nanorods in the Photoelectrode on the Efficiency of Dye Sensitized Solar Cells

**Md. Mahbubur Rahman,[†] Hyun-Yong Kim,[‡] Young-Deok Jeon,[§] In-Soo Jung,[§] Kwang-Mo Noh,[*] and Jae-Joon Lee[†,§,*]**

*Nanotechnology Research Center & Department of Nano Science and Mechatronics Engineering, Konkuk University, Chungju 380-701, Korea. [*]E-mail: kmnoh@kku.ac.kr*
*[†]Department of Advanced Technology Fusion, Konkuk University, Seoul 143-701, Korea. [*]E-mail: jjlee@kku.ac.kr*
*[‡]ENBKOREA Co. LTD., Jangyoungsil Gwan 1688-5, Daejeon 306-230, Korea*
*[§]Nanotechnology Research Center & Department of Applied Chemistry, Konkuk University, Chungju 380-701, Korea*
*Received April 23, 2013, Accepted June 26, 2013*

The effect of $TiO_2$ nanorods (TNR) and nanoparticles (TNP) composite photoelectrodes and the role of TNR to enhance the energy conversion efficiency in dye-sensitized solar cells (DSSCs) was investigated. The 5% TNR content into the TNP photoelectrode significantly increased the short-circuit current density ($J_{sc}$) and the open-circuit potential ($V_{oc}$) with the overall energy conversion efficiency enhancement of 13.6% compared to the pure TNP photoelectrode. From the photochemical and impedemetric analysis, the increased $J_{sc}$ and $V_{oc}$ for the 5% TNR/TNP composite photoelectrode was attributed to the scattering effect of TNR, reduced electron diffusion path and the suppression of charge recombination between the composite photoelectrode and electrolyte or dye.

**Key Words :** Dye-sensitized solar cell, $TiO_2$ nanorod, Composite photoelectrode, Scattering effect, Recombination

## Introduction

Dye-sensitized solar cells (DSSCs) have attracted enormous interest over the last two decades due to its high efficiency, low cost and simple preparation procedure.[1,2] In general, titanium di-oxide ($TiO_2$) nanoparticle (TNP)-based photoelectrode with mesoporous structure and anatase crystalline polymorph has been applied as an efficient electron transport medium in DSSC.[3,4] $TiO_2$ has been used extensively in DSSCs due to its oxygen vacancies, titanium interstitials and high surface area.[3] Additionally, $TiO_2$ is non-toxic and abundant in nature. However, the structural disorder of TNP film induced the elongation of electron diffusion length and ultrafast scattering of free electron, which increased the recombination probability between the TNP and electrolyte or dye.[5,6] This increased recombination probability in the TNP film reduced the electron collection efficiency and limits the energy conversion efficiency in DSSCs.

In recent years, various one dimensional (1D) $TiO_2$ nanostructures such as nanotube, nanorod, nanofiber and nanowire have been utilized as an efficient photoelectrode material in DSSCs.[7-10] This is because 1D nanostructures could effectively decrease the electron collecting path and increase the collection efficiency with reduced recombination.[3,11] Moreover, light scattering effect is also anticipated with the 1D nanostructures.[3] Most of these studies were applied for only pure 1D nanostructured film. Few studies reported the effect of 1D nanostructure/TNP composite film in DSSC photoelectrode to combine the advantages of each other.

In this work, the effect of TNR/TNP composites with different composition of synthesized TNR into the commercially available TNP on the performance of DSSCs has been investigated. The optimal percentage of the TNR incorporation into the TNP photoelectrodes for improved energy conversion was proposed based on the optical, photoelectrochemical, and impedemetric analysis.

## Experimental

**Synthesis of TNR.** The TNR was synthesized by mixing 20 mL of titanium(IV) isopropoxide (TTIP) (Sigma-Aldrich) in 100 mL ethanol with stirring followed by the addition of 0.5 M KOH. The mixture was refluxed for 2 h with Zirconia balls under stirring condition. The mixture was further refluxed for 24 h with the addition of 50 mL water. The precipitates collected, by centrifuge method, were washed with water and ethanol and dried for 24 h at room temperature. The as-synthesized sample was calcinated at 500 °C for 30 min in an electric muffle furnace under ambient condition before further characterization.

**Preparation of TNR/TNP Composite Paste.** The detailed procedure for the preparation of TNR/TNP composite paste was described in our previous reports.[4,7] Briefly, 1.0 g of TNP (TTP-20N, ENBKOREA Co., Ltd., Korea, particle size 20 nm) was pre-treated with acetyl-acetone and as-synthesized TNRs were mixed (TNR composition 0, 0.5, 5, 15 and 20%) separately with 2 mL of distilled water, 0.05 mL of acetyl-acetone, 5 mL of 10% ethanolic solution of hydroxypropyl cellulose (HPC), and 5 mL of ethanol with vigorous stirring. Then, the mixture was stirred continuously for 12 h. Finally, ethanol was evaporated slowly at 50 °C with constant stirring to get the viscous paste in which cellulose was 50%

(w/w).

**Fabrication of DSSCs.** The TNP and TNR/TNP composite films on fluorine-doped tin oxide (FTO, Pilkington, 8 Ω/sq., USA) glasses were prepared by screen printing method and the as-prepared electrodes were sintered at 500 °C for 30 min in an electric muffle furnace under ambient condition. The sintered films were dipped into a 0.3 mM ethanolic solution of *cis*-diisothiocyanato-bis(2,2'-bipyridyl-4,4'-dicarboxylato) ruthenium(II) bis-tetrabutylammonium (N719) dye for 20 h. The platinum (Pt) counter electrodes were prepared by spin coating of 5 mM ethanolic solution of chloroplatinic acid hexahydrate ($H_2PtCl_6 \cdot 6H_2O$) on FTO glass and sintered at 380 °C for 20 min in an electric muffle furnace. The dye-loaded photoelectrodes (active area *ca.* 0.09 $cm^2$) and the Pt counter electrodes were sandwiched by using 50 μm thick Surlyn film as a spacer and sealing agent under the condition of 110 °C for 10 min. The electrolyte solution having composition of 0.6 M 1,2-dimethyl-3-propylimidazolium iodide (DMPII), 0.1 M LiI, 0.1 M $I_2$, and 0.5 M 4-*tert*-butylpyridine (*tBP*) in 3-methoxypropionitrile (MPN) was injected into the cell through the drilled holes on the counter electrode. They were sealed with a transparent scotch tape for temporal sealing.

**Instrumentation.** The surface morphology of the as-synthesized TNR and as-received TNP was characterized by a scanning electron microscope (SEM, Hitachi S-3000N, Japan). The crystalline structure of the samples was analyzed by a X-ray Diffractometer (Philips, X'pert, Netherland) with Cu Kα radiation of λ = 0.15406 nm in the scanning range from 2θ = 20° to 60°. UV-Visible absorption and transmission spectra of the photoelectrodes were measured by a UV-Vis spectrophotometer (Scinco, S-3100, Korea). An AM1.5 solar simulator with a 200 W Xenon lamp (Polaronix® K201, McScience, Korea) was used to illuminate the cells, whose current density-voltage (*J-V*) properties were measured using a photovoltaic power meter (Polaronix® K101 LAB20, McScience, Korea). The incident light intensity was adjusted to 100 $mWcm^{-2}$ (1 sun) by a standard mono-Si solar cell (PVM 396, PV Measurement Inc, USA), which was certified by the U.S. National Renewable Energy Laboratory. Incident photon-to-current conversion efficiency (IPCE) spectra were carried out by IPCE measurement system (McScience, K3100 Spectral IPCE Measurement System, Polaronix®) with 300 W Xenon light source. The intensity of the incident monochromatic light was also calibrated with the same standard mono-Si solar cell (PVM 396, PV Measurement Inc, USA). Electrochemical impedance spectra (EIS) were obtained under open circuit and dark conditions in the frequency range of $10^5$ -0.1 Hz with a 5 mV ac amplitude (IM6ex, Zahner-Elektrik GmbH & Co. KG, Germany). The measured spectra were fitted to an equivalent circuit appropriate for DSSCs using Zview software (version 3.1, Scribner Associates Inc., U.S.A.).

## Result and Discussion

### Nanostructure and Crystalline Phase Analysis of TNP and TNR.

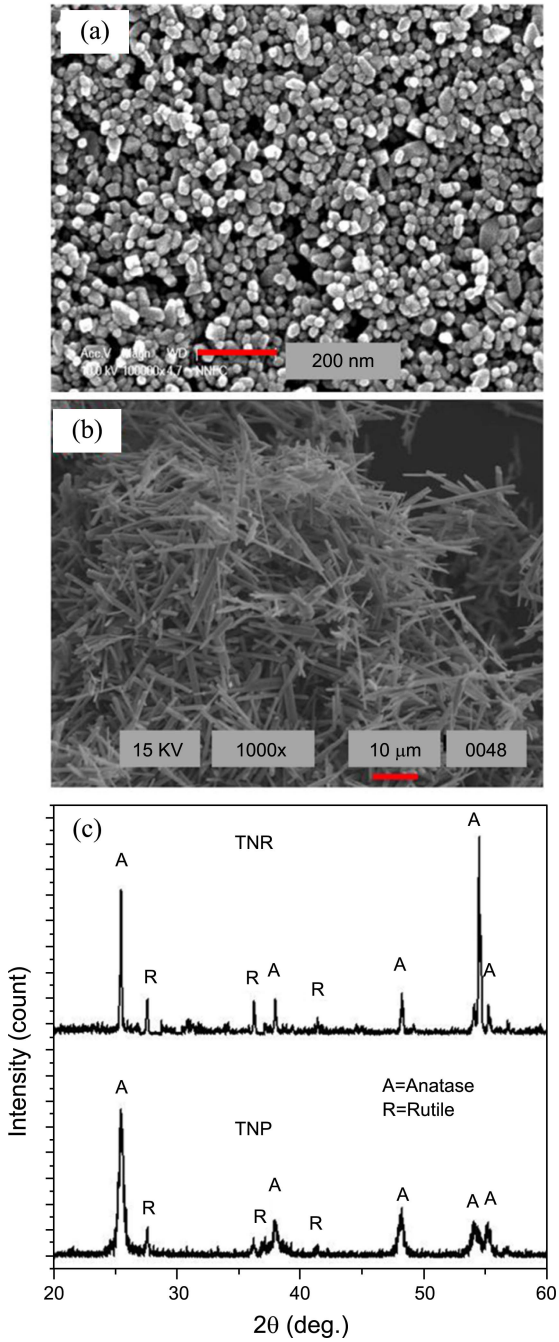


**Figure 1.** Scanning electron microscope images of (a) TNP, (b) TNR and (c) X-ray diffraction pattern of the TNP and the TNR after calcined at 500 °C.

Figure 1(a) and 1(b) show the SEM images of the as-received TNP and as-synthesized TNR, respectively. The TNP appeared as spherical in shape with an average particle size of *ca.* 20 nm. It was clearly observed that the synthesized TNRs were in the nanorod forms having very narrow size distribution. The length and diameter of the nanorods were *ca.* 200-1000 nm and *ca.* 20-100 nm, respectively. The XRD patterns of the as-received TNP and the as-synthesized TNR after calcined at 500 °C are depicted in Figure 1(c). It is clearly seen that the TNP and the TNR comprise the mixture

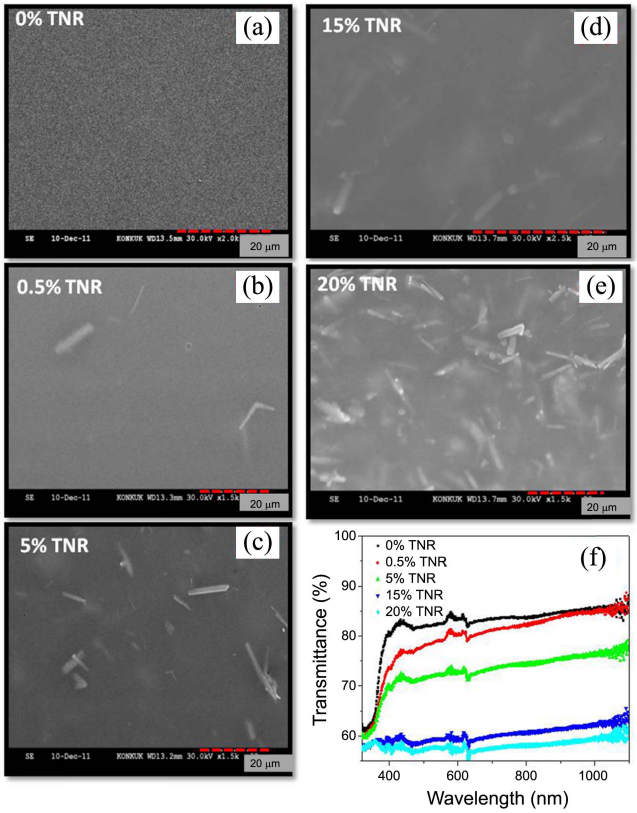


**Figure 2.** Low-magnification SEM images (top view) of different percents (%) of TNR incorporated TNP photoelectrodes (a-e) and their corresponding transmittance spectra (f).

of anatase and rutile phases with the prominent anatase phases peaked at (101), (004), (200), (105) and (211).

**SEM and Transmittance Characteristics of Composite Photoelectrodes**. Figure 2(a-e) show the top view SEM images of different percentages of TNR/TNP composite photoelectrodes with the film thicknesses of *ca.* 10 μm for all photoeelctrodes, which revealed the gradual incorporation of TNR into TNP. Even though the surface inhomogeneity of composite films were increased with the increase of the TNR content, all the composite films were free from crack and their compactness were almost unaltered. The significantly increased inhomogeneities for high TNR content photoelectrodes were attributed to the differences in the interfacial characteristics of TNR and TNP.[12] Although, the increased inhomogeneity of the photoelectrode film decreased the DSSCs performance, the increased porosity is crucial for enhanced photoconversion efficiency. Therefore, investigation of the optimum percent of TNR into TNP for enhancing the efficiency is an important strategy.

Figure 2(f) shows that the transmittance decreases at every wavelength (300-1100 nm) with the increase of the TNR content. It demonstrated that the high TNR content into TNP increased the photon absorption capacity and it was significantly higher for 15 and 20% TNR content. This further established that the TNR has the high ability to scatter light and prolong the optical path length,[13] which is favorable for extra light harvesting of lower energy photon of the adsorbed dyes and corroborates to enhance the photo-current.

**Photovoltaic Characteristics of the DSSC Photoelectrodes.** Table 1 summarizes the photovoltaic parameters of the photoelectrodes constructed by different amount of TNR incorporated TNP. It was observed that the open-circuit potential ($V_{oc}$) increased with the increasing percentage (%) of the TNR contents, while $J_{sc}$ increased for 0.5 and 5% TNR/TNP composite photoelectrodes and decreased with the further incorporation of TNR, *i.e.* for 15 and 20% TNR/TNP composite photoelectrodes. The addition of nanorods in the film improved the overall energy conversion efficiencies *ca.* 3.2 and 13.6% for 0.5 and 5% TNR/TNP composite photoelectrodes, respectively, compared to that of the pure TNP photoelectrode. The 5% TNR/TNP composite photoelectrode presented highest performance compared to all other electrodes with a $J_{sc}$ of 11.06 mA/cm$^2$, $V_{oc}$ of 0.767 V and an overall conversion efficiency ($\eta$) of 6.02%. The significantly improved $J_{sc}$ for 5% TNR/TNP composite photoelectrode (Fig. 3(a)) was attributed to the directional electron movement along the nanorod axis due to its 1D channel, which facilitates the carrier transportation, thereby reducing the electron losses incurred by charge-hopping across the grain boundaries[14] and greater fraction of light scattering within the film caused by TNR. The $J_{sc}$ value agreed well with the results obtained in the IPCE spectra (Fig. 3(b)). The 15 and 20% TNR/TNP composite photoelectrodes showed decreased values of $J_{sc}$. This could be due to lower dye loading capacity of the film as summarized in Table 1. All the TNR/TNP composite photoelectrodes showed higher $V_{oc}$ compared to TNP photoelectrode, which might be due to the suppression of electron recombination in the composite photoelectrodes.

**Impedemetric Characteristics of the Photoelectrodes.** Electrochemical impedance spectroscopy (EIS) was applied to investigate the kinetics of the electron transfer processes at the photoelectrode/electrolyte interface. The Bode phase plot of EIS spectra are presented in Figure 3(c) (for 5%

**Table 1.** Photovoltaic and kinetic parameters of different DSSCs photoelectrodes along with their amount of adsorbed dye

| TNR content (%) into TNP photoelectrodes | $J_{sc}$ (mA/cm$^2$) | $V_{oc}$ (V) | *FF* (%) | $\eta$ (%) | $k_{T/E}$ ($s^{-1}$) | $\tau_{eff}$ (ms) | Adsorbed dye amount × $10^{-7}$ (mol/cm$^2$) |
|---|---|---|---|---|---|---|---|
| 0% TNR | 9.93 | 0.740 | 71.57 | 5.30 | 77.23 | 2.06 | 2.43 |
| 0.5% TNR | 10.36 | 0.758 | 69.76 | 5.47 | 54.96 | 2.90 | 2.27 |
| 5% TNR | 11.06 | 0.767 | 70.97 | 6.02 | 38.70 | 4.11 | 2.24 |
| 15% TNR | 9.71 | 0.772 | 71.15 | 5.33 | 36.98 | 4.31 | 2.22 |
| 20% TNR | 8.86 | 0.774 | 71.33 | 4.90 | 25.58 | 6.21 | 2.19 |

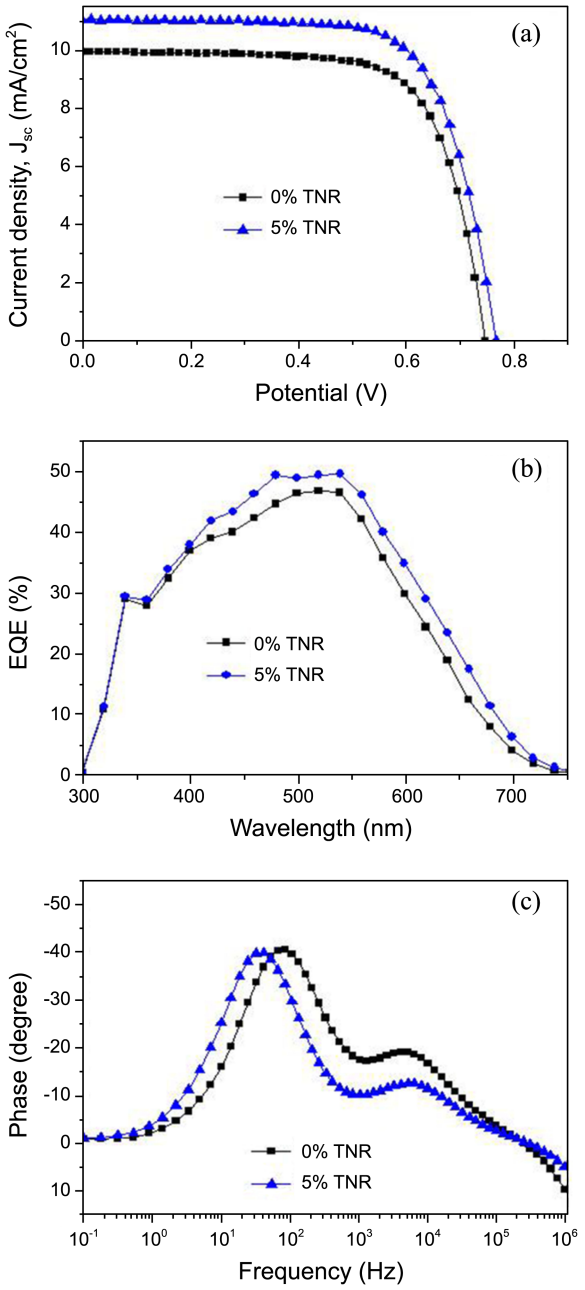


**Figure 3.** Comparison of current density-voltage (*J-V*) (a), Incident photon-to-current conversion efficiencies (IPCE) (b), and the Bode plots from electrochemical impedance measurement under dark and open circuit condition (c) for 0% and 5% TNR/TNP photoelectrodes of DSSCs.

TNR/TNP and TNP only) and the calculated kinetic parameters of all the composite photoelectrodes were summarized in Table 1. The recombination rate ($k_{T/E}$) and electron life time ($\tau_{eff}$) in the photoelectrode was estimated from the mid-frequency peak as $\omega_{max} = k_{T/E}$ and $\tau_{eff} = 1/2\pi\ \omega_{max}$, respectively.[15,16] It is clearly observed from the Table 1 that the $k_{T/E}$ value decreases with the increasing percentage of TNR content. These lower $k_{T/E}$ values strongly suggested the lower electron recombination in composite photoelectrodes compared to that of the TNP photoelectrode and the recombination is the least for 20% TNR contents, which is consistent with the variation of $V_{oc}$. The $\tau_{eff}$ in the photoelectrodes increases with the increasing amount of TNR percentage, which confirms that the electron transportation is facilitated by the 1D characteristic of TNR.[17]

## Conclusions

In this work, the effect of the TNR into TNP photoelectrode was investigated based on the electrochemical and photochemical point of view. Results demonstrated that the optimal percent of the TNR incorporation into the TNP photoelectrodes for improved DSSC efficiency was 5%, which increased the $J_{sc}$ value by 11.38% compared to that of pure TNP electrode. The increased $J_{sc}$ for 5% TNR composite photoelectrode was attributed to the improved electron collection efficiency and light scattering effect due to the addition of TNR. The $V_{oc}$ of all the composite photoelectrodes increased with increasing percentage of TNR. The improved $V_{oc}$ of all the composite photoelectrodes could be due to suppression of electron recombination at the photoelectrode/electrolyte interface.

**Acknowledgments.** This paper was supported by Konkuk University in 2012.

## References

1. Grätzel, M. *Nature* **2001**, *414*, 338.
2. Wu, J. H.; Lan, Z.; Lin, J. M.; Huang, M.; Hao, S.; Sato, T.; Yin, S. *Adv. Mater.* **2007**, *19*, 4006.
3. Lee, J.-J.; Rahman, M. M.; Sarker, S.; Nath, N. C. D.; Ahammad, A. J. S.; Lee, J. K. In *Composite Materials for Medicine and Nanotechnology*; Attaf, B., Ed.; InTech: Croatia, 2011; p 181.
4. Rahman, M. M.; Son, H.-S.; Lim, S.-S.; Chung, K.-H.; Lee, J.-J. *J. Electrochem. Sci. Technol.* **2011**, *2*, 110.
5. Wang, Z. S.; Kawauchi, H.; Kashima, T.; Arakawa, H. *Coord. Chem. Rev.* **2004**, *248*, 1381.
6. Gong, D.; Grimes, C. A.; Varghese, O.; Hu, W.; Singh, R. S.; Chen, Z.; Dickey, E. C. *J. Mater. Res.* **2001**, *16*, 3331.
7. Chung, K.-H.; Rahman, M. M.; Son, H.-S.; Lee, J.-J. *Int. J. Photoenergy* **2012**, 2012, Article ID 215802, 6 pages.
8. Song, K.; Jang, I.; Oh, S.-G. *Bull. Korean Chem. Soc.* **2013**, *34*, 355.
9. Jiu, J.; Isoda, S.; Wang, F.; Adachi, M. *J. Phys. Chem. B* **2006**, *110*, 2087.
10. Yang, L.; Leung, W. W.-F. *Adv. Mater.* **2011**, *23*, 4559.
11. Macak, J. M.; Zlamal, M.; Krysa, J.; Schmuki, P. *Small* **2007**, *3*, 300.
12. Kontos, A. I.; Kontos, A. G.; Tsoukleris, D. S.; Bernard, M.-C.; Spyrellis, N.; Falaras, P. *J. Mater. Process. Technol.* **2008**, *196*, 243.
13. Brüggemann, B.; Organero, J. A.; Pascher, T.; Pullerits, T.; Yartsev, A. *Phys. Rev. Lett.* **2006**, 97, Article ID 208301, 4 pages.
14. Mohamed, A. E. R.; Rohani, S. *Energy Environ. Sci.* **2011**, *4*, 1065.
15. Adachi, M.; Sakamoto, M.; Jiu, J.; Ogata, Y.; Isoda, S. *J. Phys. Chem. B* **2006**, *110*, 13872.
16. Yu, Z.; Vlachopoulos, N.; Gorlov, M.; Kloo, L. *Dalton Trans.* **2011**, *40*, 10289.
17. Pommer, E. E.; Liu, B.; Aydil, E. S. *Phys. Chem. Chem. Phys.* **2009**, *1*, 9648.